Nucleon Electromagnetic Form Factors

Kees de Jager

Jefferson Lab, Newport News, VA 23606, USA

1 Introduction

Although nucleons account for nearly all the visible mass in the universe, they have a complicated structure that is still incompletely understood. The first indication that nucleons have an internal structure, was the measurement of the proton magnetic moment by Frisch and Stern (1933) which revealed a large deviation from the value expected for a point-like Dirac particle. The investigation of the spatial structure of the nucleon, resulting in the first quantitative measurement of the proton charge radius, was initiated by the HEPL (Stanford) experiments in the 1950s, for which Hofstadter was awarded the 1961 Nobel prize. The first indication of a non-zero neutron charge distribution was obtained by scattering thermal neutrons off atomic electrons. The recent revival of its experimental study through the operational implementation of novel instrumentation has instigated a strong theoretical interest.

Nucleon electro-magnetic form factors (EMFFs) are optimally studied through the exchange of a virtual photon, in elastic electron-nucleon scattering. The momentum transferred to the nucleon by the virtual photon can be selected to probe different scales of the nucleon, from integral properties such as the charge radius to scaling properties of its internal constituents. Polarization instrumentation, polarized beams and targets, and the measurement of the polarization of the recoiling nucleon have been essential in the accurate separation of the charge and magnetic form factors and in studies of the elusive neutron charge form factor.

2 Theory of Electron Scattering and Form Factor Measurements

The nucleon EMFFs are of fundamental importance for the understanding of the nucleon's internal structure. Under Lorentz invariance, spatial symmetries and charge conservation, the most general form of the electromagnetic current inside a nucleon can be written as:

$$J^{\mu}_{EM} = F_1(Q^2)\gamma^{\mu} + \frac{\kappa}{2M_N}F_2(Q^2)i\sigma^{\mu\nu}q_{\nu}, \tag{1}$$

where F_1 denotes the helicity non-flip Dirac form factor, F_2 the helicity flip Pauli form factor, $Q^2 = -q^2$, and κ the nucleon anomalous magnetic moment. The remaining variables are defined in Figure 1. The second term, usually referred to as the Foldy contribution, carries the information about the nucleon anomalous magnetic moment and thus is of relativistic origin. It is useful to introduce the isospin form-factor components, corresponding to the isoscalar (s) and isovector (v) response of the nucleon,

$$F_i^s = \frac{1}{2}(F_i^p + F_i^n); \quad F_i^v = \frac{1}{2}(F_i^p - F_i^n); \quad (i = 1, 2). \tag{2}$$

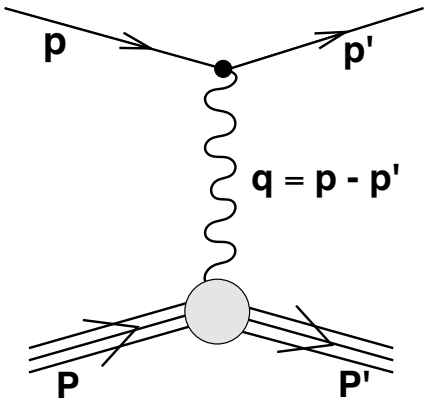

Figure 1. *The Feynman diagram for the scattering of an electron with four-momentum $p = (E_e, \vec{p})$ through an angle θ_e off a nucleon with mass M_N and four-momentum P. In this diagram a single virtual photon with four-momentum $q = p - p' = (\omega, \vec{q})$ is exchanged. The four-momenta of the scattered electron and nucleon are $p' = (E'_e, \vec{p'})$ and P', respectively.*

The form factors can be continued analytically into the complex plane and can be related in different regions through a dispersion relation of the form

$$F(t) = \frac{1}{\pi}\int_{t_0}^{\infty}\frac{\mathrm{Im}\,F(t')}{t' - t}dt', \tag{3}$$

with $t = -Q^2$, $t_0 = 9(4)M_\pi^2$ for the isoscalar (isovector) case and M_π the pion mass. In the isovector case the minimum t-value is determined by the threshold for the $e^+e^- \rightarrow \pi^+\pi^-$ reaction, in the isovector case the lightest hadronic state involves three pions. In the positive Q^2-region, called spacelike, form factors can be measured through electron scattering, in the negative Q^2-region, called timelike, form factors can only be measured through the creation or annihilation of a $N\bar{N}$-pair.

In the plane wave born approximation the cross section for elastic electron-nucleon scattering can be expressed in the Rosenbluth (1950) formula as:

$$\frac{d\sigma}{d\Omega} = \sigma_M[(F_1^2 + \kappa^2\tau F_2^2) + 2\tau(F_1 + \kappa F_2)^2 \tan^2(\frac{\theta_e}{2})], \tag{4}$$

where $\tau = Q^2/(4M_N^2)$ and $\sigma_M = (\frac{\alpha_{QED}\cos\theta_e/2}{2E_e \sin^2\theta_e/2})^2 \frac{E'_e}{E_e}$ is the Mott cross section for scattering off a point-like particle, with α_{QED} denoting the fine-structure constant. The remaining variables are defined in Figure 1. F_1 and F_2 are now clearly identified as the Dirac and Pauli form factors. Hofstadter determined the values of F_1 and F_2 by measuring the cross section at different scattering angles, but the same value of Q^2 and drawing intersecting ellipses. Hand, Miller and Wilson (1963) expressed eq. 4 in an alternate form

$$\frac{d\sigma}{d\Omega} = \sigma_M[\frac{(G_E^p)^2 + \tau(G_M^p)^2}{1+\tau} + 2\tau(G_M^p)^2 \tan^2(\frac{\theta_e}{2})] = \frac{\sigma_M}{\epsilon}[\tau(G_M^p)^2 + \epsilon(G_E^p)^2](\frac{1}{1+\tau}), \tag{5}$$

with $\epsilon = 1/[1 + 2(1+\tau)\tan^2(\frac{\theta_e}{2})]$ the linear polarization of the virtual photon and

$$\begin{aligned} G_E(Q^2) &= F_1(Q^2) - \tau\kappa F_2(Q^2); \qquad G_E^p(0) = 1; \qquad G_E^n(0) = 0; \\ G_M(Q^2) &= F_1(Q^2) + \kappa F_2(Q^2); \quad G_M^{p,n}(0) = \mu_{p,n}, \end{aligned} \tag{6}$$

with $\mu_{p,n}$ denoting the magnetic moment of the proton and neutron, respectively. This equation illustrates that the electric and magnetic Sachs form factors G_E^p and G_M^p can be separated in a straightforward way by performing cross-section measurements at fixed Q^2 as a function of ϵ, over a range of (θ_e,E_e) combinations. This technique has become somewhat erroneously known as the Rosenbluth separation technique. In the Breit frame, which for elastic scattering is equivalent to the electron-nucleon centre-of-mass frame, the Sachs form factors can be identified with the Fourier transform of the nucleon charge and magnetization density distributions. In this frame the incoming electron has momentum $\vec{p} = +\vec{q}/2$ and hits a nucleon which has equal but opposite momentum $\vec{P} = -\vec{q}/2$. The exchanged photon carries momentum $\vec{q}$ but no energy. In the Breit frame the electromagnetic current of the proton simplifies into the following expression

$$J_{EM}^{\mu} = e\{G_E + (\vec{\sigma} \times \vec{q})G_M\}. \tag{7}$$

Through the mid-1990s practically all available proton EMFF data had been collected using the Rosenbluth separation technique. This experimental procedure requires

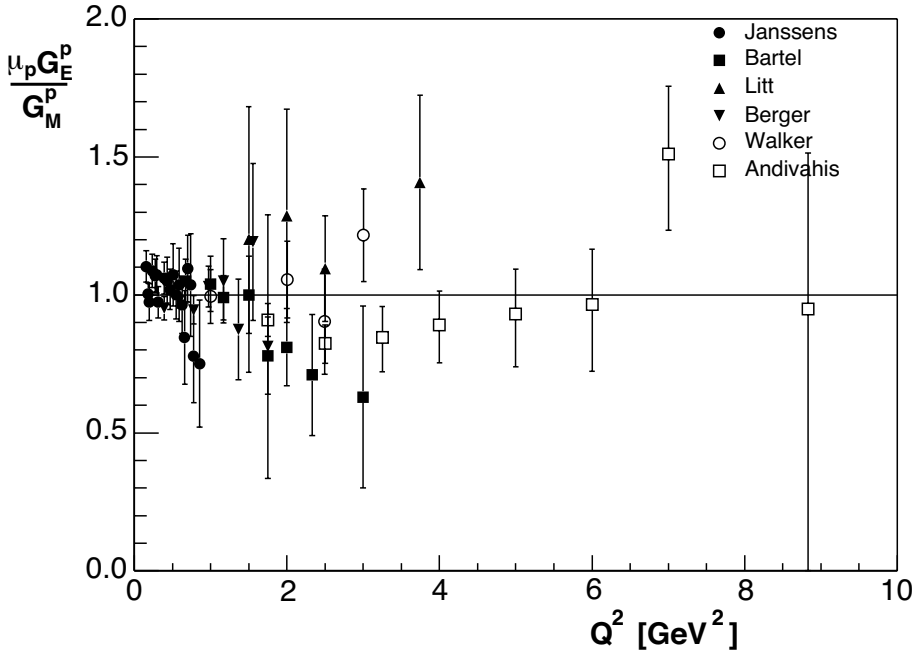

Figure 2. *The ratio $\mu_p G_E^p / G_M^p$ from Rosenbluth separation. Data are from References (Janssens et al. 1966, Bartel et al. 1966, Litt et al. 1970, Berger et al. 1971, Walker et al. 1994 and Andivahis et al. 1994). The errors shown in all figures are the quadratic sum of the statistical and systematic contributions.*

an accurate knowledge of the electron energy and the total luminosity. In addition, because the G_M^p contribution to the elastic cross section is weighted with Q^2, data on G_E^p suffer from increasing systematic uncertainties with increasing Q^2-values. The then available world data set (Bosted *et al.* 1995) was compared to the so-called dipole parametrization G_D, which corresponds to two poles with opposite sign close to each other in the time-like region. In coordinate space G_D corresponds to exponentially decreasing radial charge and magnetization densities, albeit with a non-physical discontinuity at the origin:

$$G_D = \left(\frac{\Lambda^2}{\Lambda^2 + Q^2} \right)^2 \qquad \text{with } \Lambda = 0.84 \text{ GeV and } Q \text{ in GeV}. \tag{8}$$

For G_E^p, G_M^p/μ_p and G_M^n/μ_n the available data agreed to within 20% with the dipole parametrization. Both the G_E^p and the G_M^p/μ_p data could be fitted adequately with an identical parametrization. However, the limitation of the Rosenbluth separation was evident from the fact that different data sets for $\mu_p G_E^p / G_M^p$ scattered by up to 50% at Q^2-values larger than 1 GeV^2 (Figure 2). Although no fundamental reason has been found for the success of the dipole parametrization, it is still used as a base line for comparison of data because it removes the largest variation with Q^2 and enables small differences to be seen.

3 Instrumentation for Form Factor Measurements

More than 40 years ago Akhiezer *et al.* (1958) (followed 20 years later by Arnold *et al.* (1981)) showed that the accuracy of nucleon charge form-factor measurements could be increased significantly by scattering polarized electrons off a polarized target (or equivalently by measuring the polarization of the recoiling proton). However, it took several decades before technology had sufficiently advanced to make the first of such measurements feasible and only in the past few years has a large number of new data with a significantly improved accuracy become available. The next few sections introduce the various techniques. The figure of merit for different polarization techniques is defined as the product of the luminosity, the square of the degree of polarization or analyzing power and the efficiency. For G_E^p measurements the highest figure of merit at Q^2-values larger than a few GeV^2 is obtained with a focal plane polarimeter. Here, the Jacobian focusing of the recoiling proton kinematics allows one to couple a standard magnetic spectrometer for the proton detection to a large-acceptance non-magnetic detector for the detection of the scattered electron. For studies of G_E^n one needs to use a magnetic spectrometer to detect the scattered electron in order to cleanly identify the reaction channel. As a consequence, the figure of merit of a polarized $^3\vec{\mathrm{He}}$ target is comparable to that of a neutron polarimeter.

3.1 Polarized Beam

Various techniques are available to produce polarized electron beams, but photo-emission from GaAs has until now proven to be optimal (Aulenbacher 2002). A thin layer of GaAs is illuminated by a circularly polarized laser beam of high intensity, which preferentially excites electrons of one helicity state to the conductance band through optical pumping. The helicity sign of the laser beam can be flipped at a rate of tens of Hertz by changing the high voltage on a Pockels cell. The polarized electrons that diffuse to the photocathode surface are then extracted by a 50-100 kV potential. An ultra-high vacuum environment is required to minimize surface degradation of the GaAs crystal by backstreaming ions. Initially, the use of bulk GaAs limited the maximum polarization to 50% because of the degeneracy of the $P_{3/2}$ sublevels. This degeneracy is removed by introducing a strain in a thin layer of GaAs deposited onto a thicker layer with a slightly different lattice spacing. Although such strained GaAs cathodes have a significantly lower quantum efficiency than bulk GaAs cathodes, this has been compensated by the development of high-intensity diode or Ti-sapphire lasers. Polarized electron beams are now reliably available with a polarization close to 80% at currents of ≥ 100 μA.

The polarized electrons extracted from the GaAs surface are first pre-accelerated and longitudinally bunched and then injected into an accelerator. Typically, the polarization vector of the electrons is manipulated in a Wien filter, a system of crossed magnetic and electric fields and magnetic quadrupole lenses, so that the electrons are fully longitudinally polarized at the target. If the beam is injected into a storage ring for use with an internal target, a Siberian snake (Derbenev and Kondratenko 1973) is needed to compensate for the precession of the polarization.

Three processes are used to measure the beam polarization: Mott (Steigerwald 2001)

scattering, Møller (Hauger *et al.* 2001) scattering or Compton (Baylac *et al.* 2001) scattering. Any of these results in a polarimeter with an accuracy approaching 1%. In a Mott polarimeter the beam helicity asymmetry is measured in scattering polarized electrons off atomic nuclei. This technique is limited to electron energies below $\sim$ 20 MeV and multiple scattering effects have to be estimated by taking measurements at different target foil thicknesses. In a Møller polarimeter polarized electrons are scattered off polarized atomic electrons in a magnetized iron foil. In this technique the major uncertainties are in the corrections for atomic screening and in the foil magnetization, unless the polarizing field is strong enough to fully saturate the magnetization. A potentially superior alternative (Chudakov and Luppov 2004) has been proposed in which the electrons are scattered off a sample of atomic hydrogen, polarized to a very high degree in an atomic beam, and trapped in a superconducting solenoid. Finally, in a Compton polarimeter the beam helicity asymmetry is measured in scattering polarized electrons off an intense beam of circularly polarized light, produced by trapping a laser beam in a high-finesse Fabry-Perot cavity. The electron beam in a storage ring is sufficiently intense that a laser beam can be directly scattered off the electron beam without the use of an amplifying cavity. Only the last two methods, the atomic hydrogen Møller and the Compton polarimeter, have no effect on the quality of the electron beam and thus can be used continuously during an experiment.

3.2 Polarized Targets

In polarized targets for protons two different techniques are used, depending on the intensity of the electron beam. In storage rings where the circulating beam can have an intensity of 100 mA or more, but the material interfering with the beam has to be minimized, gaseous targets are used, whereas in external targets solid targets can be used. Because free neutrons are not available in sufficient quantity, effective targets, such as deuterium or ^{3}He, are necessary, and the techniques used to polarize the deuteron are similar to those used for the proton. For ^{3}He gaseous targets are used both in internal and external targets.

Solid polarized targets that can withstand electron beams with an intensity of up to 100 nA all use the dynamic nuclear polarization technique (Crabb *et al.* 1995). A hydrogenous compound, such as NH_3 or LiD, is doped, e.g. by radiation damage, with a small concentration of free radicals. Because the occupation of the magnetic substates in the radicals follows the Boltzmann distribution, the free electrons are polarized to more than 99% in a $\sim$ 5 T magnetic field and at a $\sim$ 1 K temperature (see Figure 3). A radiofrequency (RF) field is then applied to induce transitions to states with a preferred orientation of the nuclear spin. Because the relaxation time of the electrons is much shorter than that of the nuclei, polarized nuclei are accumulated. This technique has been successful in numerous deep-inelastic lepton scattering and nucleon form-factor experiments; it has provided polarized hydrogen or deuterium targets with an average polarization of $\sim 80\%$ or $\sim 30\%$, respectively.

Internal hydrogen/deuterium targets (Steffens and Haeberli 2003) are polarized by the atomic beam source (ABS) technique, which relies on Stern-Gerlach separation and RF transitions (see Figure 4). First, a beam of atoms is produced in an RF dissociator through a nozzle cooled with liquid nitrogen. Then, atoms with different electron spin

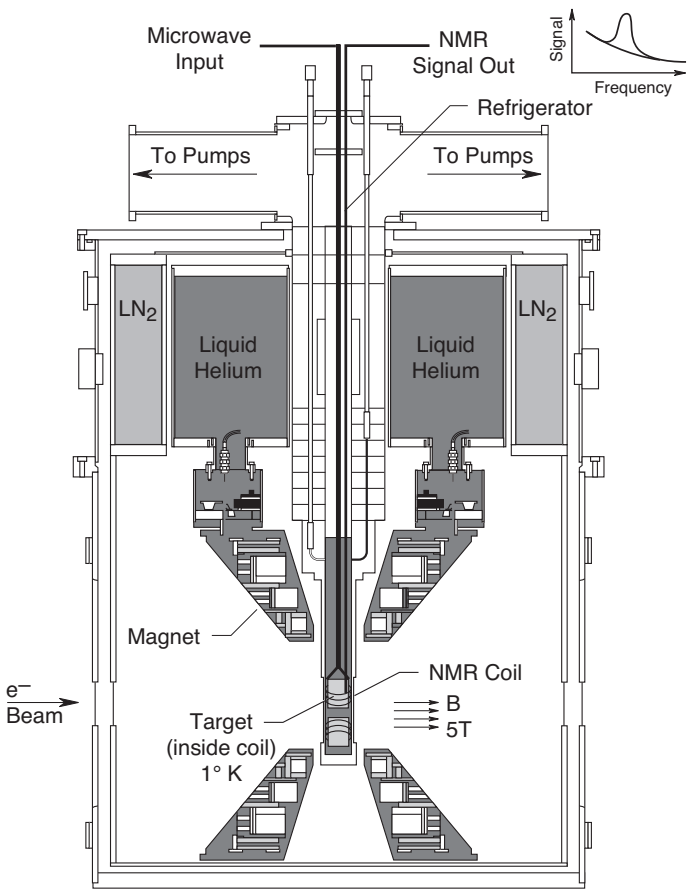

Figure 3. *Lay-out of a polarized hydrogen/deuterium target using the dynamic nuclear polarization technique.*

direction are separated through a series of permanent (or superconducting) sextupole magnets and transitions between different hyperfine states are induced by a variety of RF units (MFT/SFT/WFT). The result is a highly polarized beam with a flux up to 10^{17} atoms/s. This beam is then fed into an open-ended storage cell, which is cooled and coated to minimize recombination of the atoms bouncing off the cell walls. The circulating electron beam, passing through the long axis of the storage cell, encounters only the flowing atoms. The polarization vector is oriented with a set of coils, producing a field of ~ 0.3 T in order to minimize depolarization by the RF structure of the circulating electron beam. The diameter of the storage cell is determined by the halo of the electron beam. A target thickness of 2×10^{14} nuclei/cm^2 has been obtained at a vector polarization of more than 80%.

Polarized hydrogen or deuterium atoms can also be produced by spin-exchange collisions between such atoms and a small admixture of alkali atoms that have been polarized by optical pumping. The nucleus is then polarized in spin-temperature equilibrium. Although the nuclear polarization obtained in such a laser driven source (LDS) is smaller

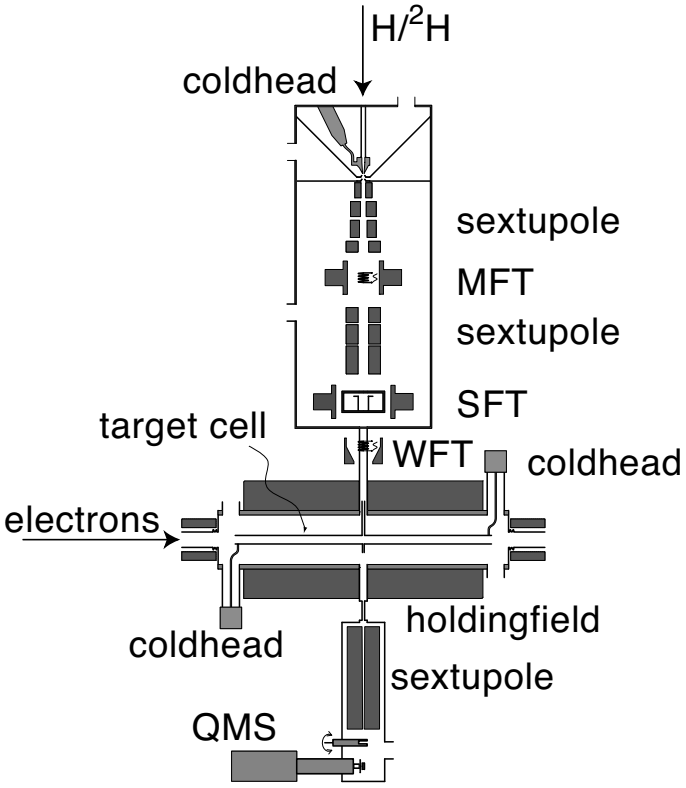

Figure 4. *Lay-out of an Atomic Beam Source target for polarized hydrogen/deuterium.*

than through the ABS technique, the flux can be more than 10^{18} atoms/s. Moreover, an LDS offers a more compact design than an ABS. A figure of merit comparable to that of the ABS at the HERMES experiment has recently been achieved by the MIT group (Clasie *et al.* 2003).

Polarized ^{3}He is attractive as an effective polarized neutron target because its ground state is dominated by a spatially symmetric s-state in which the proton spins cancel, so that the spin of the ^{3}He nucleus is mainly determined by that of the neutron. Corrections for the (small) d-state component and for charge-exchange contributions from the protons can be calculated accurately at Q^2-values smaller than 0.5 GeV^2(Golak *et al.* 2001) and larger than $\sim$ 2 GeV^2(Sargsian 2001). Direct optical pumping of ^{3}He atoms is not possible because of the energy difference between the ground state and the first excited state. Instead ^{3}He is polarized, either by first exciting the atoms to a metastable 2^3S_1 state and optically pumping that state, which then transfers its polarization to the ground state by metastability-exchange collisions, or by optically pumping a small admixture of rubidium atoms, which then transfer their polarization to the ^{3}He atoms through spin-exchange collisions (see Figure 5). In internal targets only the metastability-exchange technique has been used because of the possible detrimental effects of the rubidium admixture on the storage ring environment. With beam on target, polarization values of

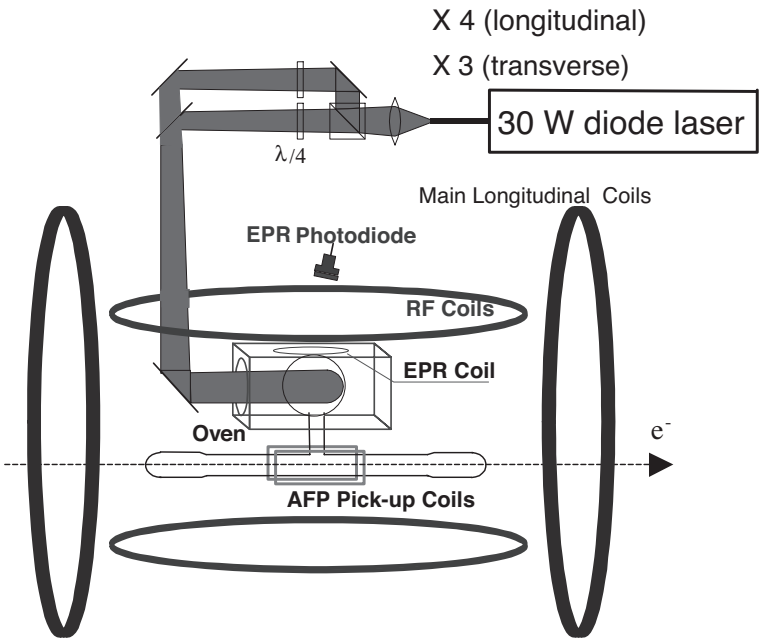

Figure 5. *Lay-out of a polarized ^{3}He target using the spin-exchange technique.*

up to 46% at target thicknesses of 1×10^{15} nuclei/cm^2 have been obtained. For external targets the spin-exchange technique (Alcorn *et al.* 2004) has been used to optically pump a glass target cell filled with 10 atm of ^{3}He with a 0.1% rubidium admixture. After the spin-exchange collisions the polarized ^{3}He diffuses into a 25 cm long cell which the electron beam traverses. Polarizations in excess of 40% have been reached with beam on target. A pair of 5 mT Helmholz coils is used to orient the polarization vector, and care must be taken to minimize depolarizing magnetic field gradients. Alternatively, the metastability technique (Surkau *et al.* 1997) has been used to polarize ^{3}He under atmospheric pressure which is then compressed to a density of more than 6 atm.

3.3 Recoil Polarimeters

Focal-plane polarimeters have long been used at proton scattering facilities to measure the polarization of the scattered proton. In such an instrument (Alcorn *et al.* 2004) the azimuthal angular distribution is measured of protons scattered in the focal plane of a magnetic spectrometer by an analyzer, which often consists of carbon. From this angular distribution the two polarization components transverse to the proton momentum can be derived

$$f(\theta, \phi) = f_0(\theta)[1 + P_n^{pol} A_y(\theta) \cos\phi + P_t^{pol} A_y(\theta) \sin\phi]. \quad (9)$$

To extract the longitudinal polarization component the nucleon's spin is precessed with a dipole magnet. The analyzer is preceded by two detectors, most often wire or

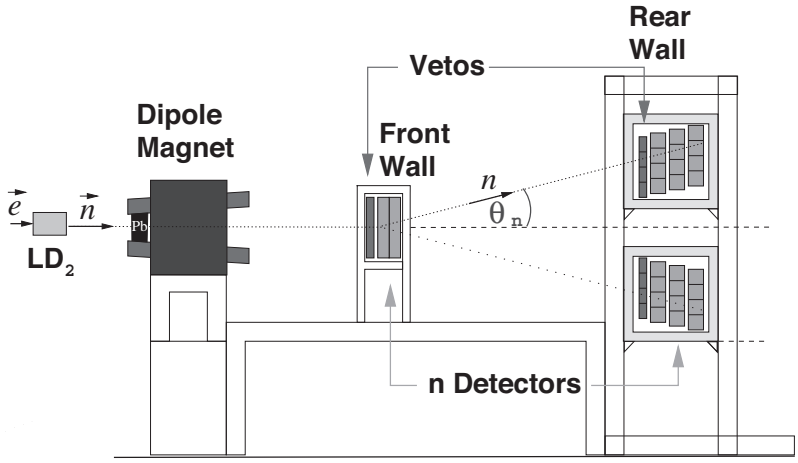

Figure 6. *Lay-out of a G_E^n measurement with a recoil polarimeter, showing the liquid deuterium target, the spin-precessing dipole magnet and the front and rear plastic scinillators.*

straw chambers, to measure the track of the incident proton; it is followed by two more detectors to track the scattered particle. The thickness of the analyzer is adjusted to the proton momentum, limiting multiple scattering while optimizing the figure of merit. In order to determine the two polarization components in the scattering plane at the target, care must be taken to accurately calculate on an event-by-event basis the precession of the proton spin in the magnetic field of the spectrometer.

Neutron polarimeters follow the same basic principle. Here, plastic scintillator material is used as an active analyzer, preceded by a veto counter to discard charged particles. This eliminates the need for the front detectors. Sets of scintillator detectors are used to measure an up-down asymmetry in the scattered neutrons, which is sensitive to a polarization component in the scattering plane, perpendicular to the neutron momentum. In modern neutron polarimeters (Ostrick *et al.* 1999) the analyzer is preceded by a dipole magnet, with which the neutron spin can be precessed (see Figure 6).

4 Experimental Results

4.1 Proton Electric Form Factor

In elastic electron-proton scattering a longitudinally polarized electron will transfer its polarization to the recoil proton. In the one-photon exchange approximation the proton can attain only polarization components in the scattering plane, parallel (P_l) and transverse (P_t) to its momentum. This can immediately be seen from the expression of the proton current in the Breit frame which separates into components proportional to G_E and G_M (see eq. 7). The ratio of the charge and magnetic form factors is directly proportional to the ratio of these polarization components:

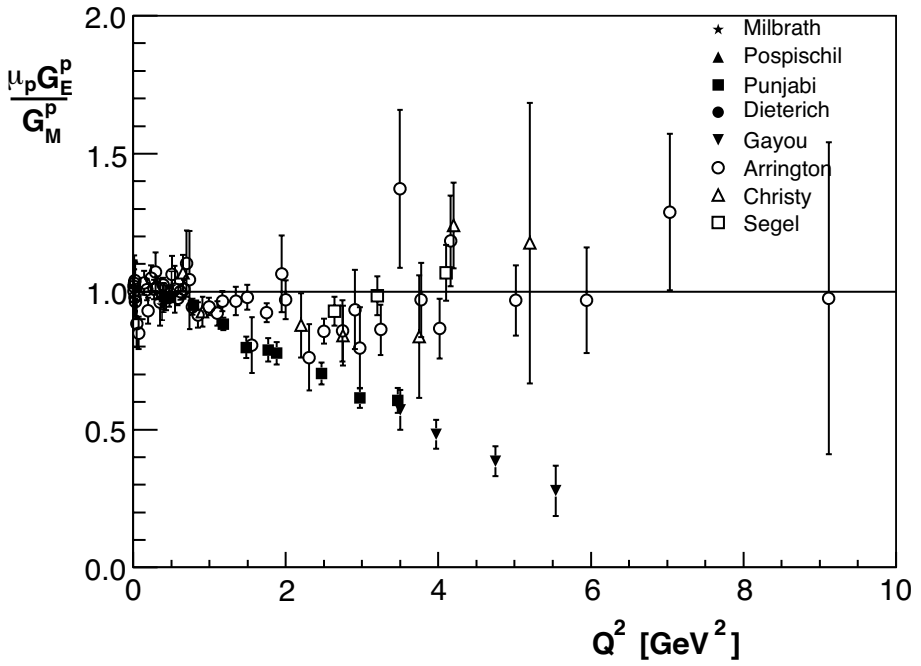

Figure 7. *The ratio $\mu_p G_E^p/G_M^p$ from polarization transfer (Milbrath et al. 1998, Pospischil et al. 2001, Punjabi et al. 2003, Dieterich et al. 2001 and Gayou et al. 2002), compared to recent Rosenbluth data (Qattan et al. 2004 and Christy et al. 2004) and the reanalysis by Arrington (2003) of older SLAC data.*

$$\frac{G_E^p}{G_M^p} = -\frac{P_t}{P_l}\frac{E_e + E_e'}{2M}\tan(\frac{\theta_e}{2}). \tag{10}$$

The polarization-transfer technique was used for the first time by Milbrath *et al.* (1998) at the MIT-Bates facility. The proton form factor ratio was measured at Q^2-values of 0.38 and 0.50 GeV^2 by scattering a 580 MeV electron beam polarized to $\sim 30\%$. A follow-up measurement was performed at the MAMI facility (Pospischil *et al.* 2001) at a Q^2-value of 0.4 GeV^2.

The greatest impact of the polarization-transfer technique was made by the two recent experiments (Punjabi *et al.* 2003, Gayou *et al.* 2002) in Hall A at Jefferson Lab, which measured the ratio G_E^p/G_M^p in a Q^2-range from 0.5 to 5.6 GeV^2. Elastic ep events were selected by detecting electrons and protons in coincidence in the two identical high-resolution spectrometers. At the four highest Q^2-values a lead-glass calorimeter was used to detect the scattered electrons in order to match the proton angular acceptance. The polarization of the recoiling proton was determined with a focal-plane polarimeter in the hadron spectrometer, consisting of two pairs of straw chambers with a carbon or polyethylene analyzer in between. The data were analyzed in bins of each of the target coordinates. No dependence on any of these variables was observed (Punjabi *et al.* 2003). Figure 7 shows the results for the ratio $\mu_p G_E^p/G_M^p$. The most striking feature of

the data is the sharp, practically linear decline as Q^2 increases:

$$\mu_p \frac{G_E^p(Q^2)}{G_M^p(Q^2)} = 1 - 0.13(Q^2 - 0.29) \quad \text{with } Q^2 \text{ in GeV}^2. \tag{11}$$

Since it is known that G_M^p closely follows the dipole parametrization, it follows that G_E^p falls more rapidly with Q^2 than G_D. This significant fall-off of the form-factor ratio is in clear disagreement with the results from the Rosenbluth extraction. Arrington (arrington1) has performed a careful reanalysis of earlier Rosenbluth data. He selected only experiments in which an adequate ϵ-range was covered with the same detector. The results (Figure 7) do not show the large scatter seen in Figure 2. Recently, Christy *et al.* (2004) analyzed an extensive data set on elastic electron-proton scattering collected in Hall C at Jefferson Lab as part of experiment E99-119. The results are evidently in good agreement with Arrington's reanalysis. Qattan *et al.* (2004) performed a high-precision Rosenbluth extraction in Hall A at Jefferson Lab, designed specifically to significantly reduce the systematic errors compared to earlier Rosenbluth measurements. The main improvement came from detecting the recoiling protons instead of the scattered electrons, so that the proton momentum and the cross section remain practically constant when one varies ϵ at a constant Q^2-value. In addition, possible dependences on the beam current are minimized. Special care was taken in surveying the angular setting of the identical spectrometer pair. One of the spectrometers was used as a luminosity monitor during an ϵ scan. Preliminary results segel of this experiment, covering Q^2-values from 2.6 to 4.1 GeV^2, are in excellent agreement with previous Rosenbluth results. This basically rules out the possibility that the disagreement between Rosenbluth and polarization-transfer measurements of the ratio G_E^p/G_M^p is due to an underestimate of ϵ-dependent uncertainties in the Rosenbluth measurements.

4.2 Two-Photon Exchange

In order to resolve the discrepancy between the results for G_E^p/G_M^p from the two experimental techniques, an ϵ-dependent modification of the cross section is necessary. In two-(or more-)photon exchanges (TPE) the nucleon undergoes a first virtual photon exchange which can lead to an intermediate excited state and then a second one or more, finally ending back in its ground state (Figure 8). The TPE contributions to elastic electron scattering have been investigated both experimentally and theoretically for the past fifty years. In the early days such contributions were called dispersive effects (Offermann *et al.* 1991). Lately, they have been relocated to radiative corrections in the so-called box diagram. Almost all analyses with the Rosenbluth technique have used radiative corrections derived by Mo and Tsai (1969) that only include the infrared divergent parts of the box diagram (in which one of the two exchanged photons is soft). Thus, terms in which both photons are hard (and which depend on the hadronic structure) have been ignored.

The most stringent tests of TPE on the nucleon have been carried out by measuring the ratio of electron and positron elastic scattering off a proton. Corrections due to TPE will have a different sign in these two reactions. Unfortunately, this (e^+e^-) data set is quite limited (Arrington 2004a), only extending (with poor statistics) up to a Q^2-value of ~ 5 GeV^2, whereas at Q^2-values larger than ~ 2 GeV^2 basically all data have been measured at ϵ-values larger than ~ 0.85. Other tests, also inconclusive, searched for

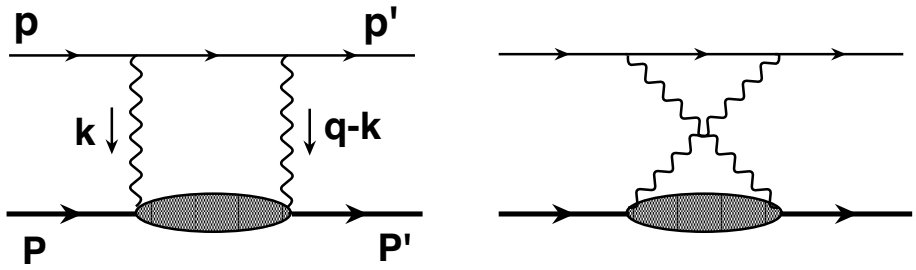

Figure 8. *The Feynman diagrams depicting two-photon exchanges.*

non-linearities in the ϵ-dependence or measured the transverse (out-of-plane) polarization component of the recoiling proton, of which a non-zero value would be a direct measure of the imaginary part of the TPE amplitude.

Several studies have provided estimates of the size of the ϵ-dependent corrections necessary to resolve the discrepancy. Because the fall-off of the form-factor ratio is linear with Q^2, and the Rosenbluth formula also shows a linear dependence of the form-factor ratio (squared) with Q^2 through the τ-term, a Q^2-independent correction linear in ϵ would cancel the disagreement. An additional constraint that any ϵ-dependent modification must satisfy, is the (e^+e^-) data set. Guichon and Vanderhaeghen (2003) introduced a general form of a TPE contribution from the so-called box diagram in radiative corrections into the amplitude for elastic electron-proton scattering. This resulted in the following modification of the Rosenbluth expression:

$$d\sigma \propto \tau + \epsilon \frac{\tilde{G_E}^2}{\tilde{G_M}^2} + 2\epsilon(\tau + \frac{\tilde{G_E}}{\tilde{G_M}})Y_{2\gamma}, \tag{12}$$

where $Y_{2\gamma} = \mathrm{Re}\,\frac{\nu \tilde{F_3}}{M^2 \tilde{G_M}}$ and $\tilde{G_M}$, $\tilde{F_2}$ and $\tilde{F_3}$ are equal to G_M, F_2 and 0, respectively, in the Born approximation. $Y_{2\gamma}$ and the "two-photon" form factors $\tilde{G_E}$ and $\tilde{G_M}$ were fitted (Guichon and Vanderhaeghen 2003) to the Rosenbluth and polarization transfer data sets. This resulted in a value of ~ 0.03 for $Y_{2\gamma}$ with very little ϵ- or Q^2-dependence.

Arrington (2004b) performed a fit to the complete data set, investigating two different modifications to the cross section with a Q^2-independent linear ϵ-dependence of 6 % over the full ϵ-range. Both modifications have the same ϵ-dependence, but one does not modify the cross section at small values of ϵ, whereas the other leaves the cross section unchanged at large values of ϵ. He found that the second gave a much better description of the complete data set. Moreover, it was in good agreement with the data set for the ratio of electron-proton and positron-proton elastic scattering.

Blunden *et al.* (2003) carried out the first calculation of the elastic contribution from TPE effects, albeit with a simple monopole Q^2-dependence of the hadronic form factors: $G(Q^2) = \Lambda^2/(Q^2 + \Lambda^2)$. They obtained a practically Q^2-independent correction factor with a linear ϵ-dependence that vanishes at forward angles ($\epsilon = 1$). However, the size of the correction only resolves about half of the discrepancy. A later calculation (W.

Melnitchouk, private communication) which used a more realistic form factor behavior, resolved up to 80% of the discrepancy.

A different approach was used by Chen *et al.* (2004), who related the elastic electron-nucleon scattering to the scattering off a parton in a nucleon through generalized parton distributions. TPE effects in the lepton-quark scattering process are calculated in the hard-scattering amplitudes. The handbag formalism of the generalized parton distributions is extended in an unfactorized framework in which the x-dependence is retained in the scattering amplitude. Finally, a valence model is used for the generalized parton distributions. The results for the TPE contribution nearly reconcile the Rosenbluth and the polarization-transfer data and retain agreement with positron-scattering data.

Hence, it is becoming more and more likely that TPE processes have to be taken into account in the analysis of Rosenbluth data and that they will affect polarization-transfer data only at the few percent level. Of course, further effort is needed to investigate the model-dependence of the TPE calculations. Experimental confirmation of TPE effects will be difficult, but certainly should be continued. The most direct test would be a measurement of the positron-proton and electron-proton scattering cross-section ratio at small ϵ-values and Q^2-values above 2 GeV^2. Positron beams available at storage rings are too low in either energy or intensity, but a measurement in the CLAS detector at Jefferson Lab, a more promising venue, has been proposed (Brooks *et al.* 2004). A measurement of the beam or target single-spin asymmetry normal to the scattering plane, which directly accesses the imaginary part of the box diagrams, would provide a sensitive test of TPE calculations. Also, real and virtual Compton scattering data can provide additional constraints on calculations of TPE effects in elastic scattering. Rosenbluth analyses have so far been restricted to simple PWBA, Coulomb distortion effects should certainly be included too. Additional efforts should be extended to studies of TPE effects in other longitudinal-transverse separations, such as proton knock-out and deep-inelastic scattering (DIS) experiments.

4.3 Proton Magnetic Form Factor

An extensive data set (Borkowski *et al.* 1975) with a good accuracy is available up to a Q^2-value of more than 30 GeV^2 from unpolarized cross-section measurements (Figure 9). Because G_M^p dominates in a Rosenbluth extraction at larger Q^2-values, the G_M^p data have only a minor sensitivity to the discrepancy between the Rosenbluth extraction and the polarization-transfer technique. Brash *et al.* (2002) have shown that the G_M^p data must be renormalized upwards by $\sim 2\%$ if one assumes the polarization-transfer data to be correct.

4.4 Neutron Magnetic Form Factor

Early data on G_M^n were extracted from inclusive quasi-elastic scattering off the deuteron. However, modeling of the deuteron wave function, required to subtract the contribution from the proton, resulted in sizable systematic uncertainties. A significant break-through was made by measuring the ratio of quasi-elastic neutron and proton knock-out from a deuterium target. This method has little sensitivity to nuclear binding effects and to fluctuations in the luminosity and detector acceptance. The basic set-up used in all such

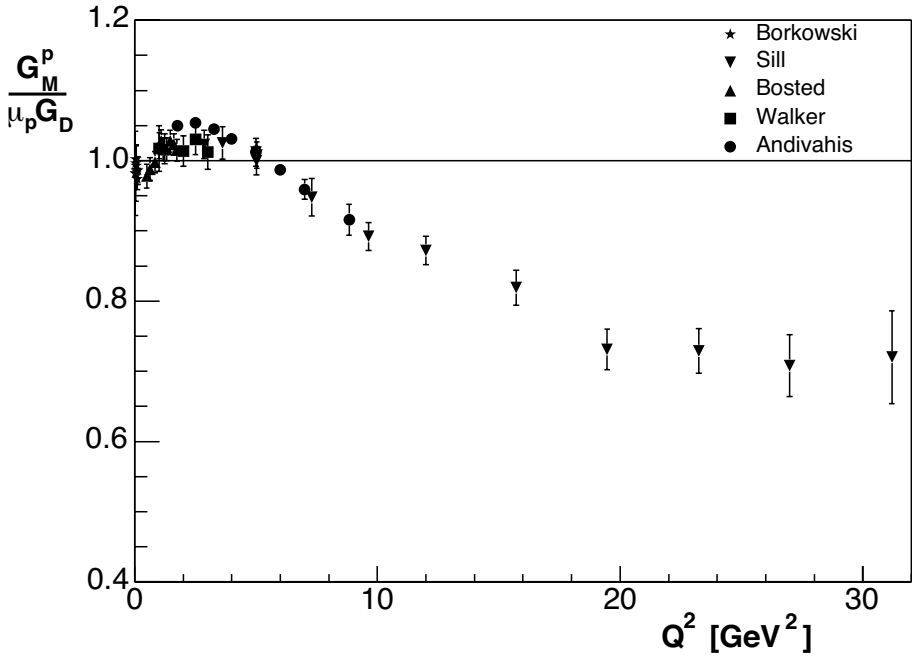

Figure 9. *The proton magnetic form factor G_M^p, in units of $\mu_p G_D$, as a function of Q^2. Data are from References (Borkowski et al. 1975, Bosted et al. 1990, Sill et al. 1993, Walker et al. 1994 and Andivahis et al. 1994).*

measurements is very similar: the electron is detected in a magnetic spectrometer with coincident neutron/proton detection in a large scintillator array. The main technical difficulty in such a ratio measurement is the absolute determination of the neutron detection efficiency. Such measurements have been pioneered for Q^2-values smaller than 1 GeV^2 at Mainz (Anklin *et al.* 1994, Anklin *et al.* 1998, Kubon *et al.* 2002) and Bonn (Bruins *et al.* 1995). The Mainz G_M^n data are 8%-10% lower than those from Bonn, at variance with the quoted uncertainty of $\sim$2%. This discrepancy would require a 16%-20% error in the detector efficiency.

A study of G_M^n at Q^2-values up to 5 GeV^2 has recently been completed in Hall B by measuring the neutron/proton quasi-elastic cross-section ratio using the CLAS detector (Brooks and Vineyard 1994). A hydrogen target was in the beam simultaneously with the deuterium target. This made it possible to measure the neutron detection efficiency by tagging neutrons in exclusive reactions on the hydrogen target. Preliminary results indicate that G_M^n is within 10% of G_D over the full Q^2-range of the experiment (0.5-4.8 GeV^2).

Inclusive quasi-elastic scattering of polarized electrons off a polarized ^{3}He target offers an alternative method to determine G_M^n through a measurement of the beam asymmetry (Donnelly and Raskin 1986)

$$A = -\frac{(\cos\theta^* v_{T'} R_{T'} + 2\sin\theta^* \cos\theta^* v_{TL'} R_{TL'})}{v_L R_L + v_T R_T}, \tag{13}$$

where θ^* and ϕ^* are the polar and azimuthal target spin angles with respect to $\vec{q}$, R_i denote various nucleon response functions, and v_i the corresponding kinematic factors. By orienting the target polarization parallel to $\vec{q}$, one measure $R_{T'}$, which in quasi-elastic kinematics is dominantly sensitive to $(G_M^n)^2$. For the extraction of G_M^n corrections for the nuclear medium (Golak *et al.* 2001) are necessary to take into account effects of final-state interactions and meson-exchange currents. The first such measurement was carried out at Bates (Gao *et al.* 1994). Recently, this technique was used to measure G_M^n in Hall A at Jefferson Lab in a Q^2-range from 0.1 to 0.6 GeV^2(Xu *et al.* 2000). This experiment provided an independent, accurate measurement of G_M^n at Q^2-values of 0.1 and 0.2 GeV^2, in excellent agreement with the Mainz data. At the higher Q^2-values G_M^n could be extracted (Xu *et al.* 2003) in plane wave impulse approximation, since final-state interaction effects are expected to decrease with increasing Q^2.

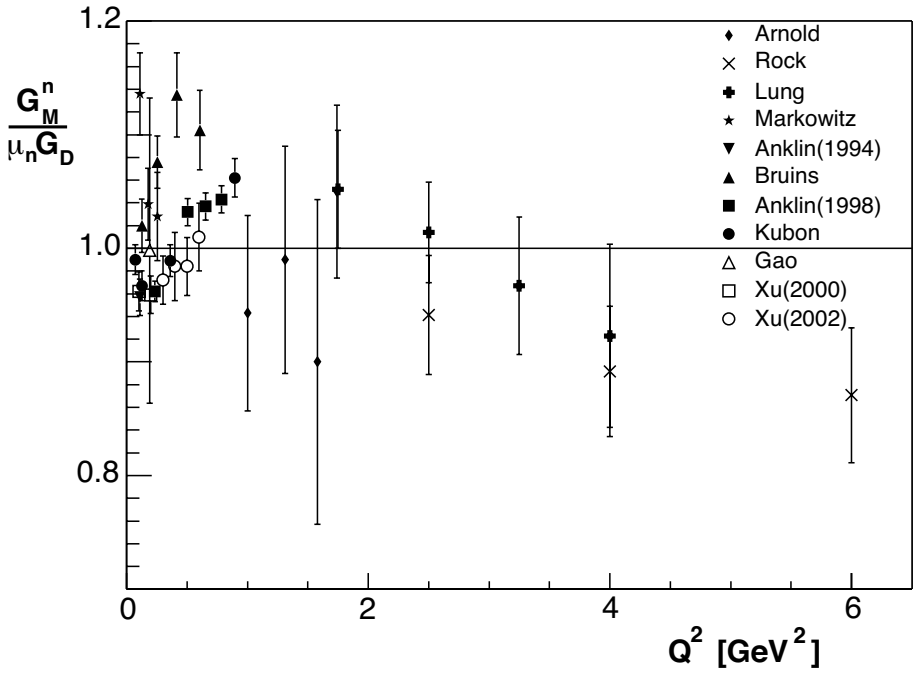

Figure 10. *The neutron magnetic form factor G_M^n, in units of $\mu_n G_D$, as a function of Q^2. Results from $^3\vec{\mathrm{He}}$ are indicated by open symbols. Data are from References (Arnold et al. 1988, Rock et al. 1992, Lung et al. 1993, Markowitz et al. 1993, Anklin et al. 1994, Bruins et al. 1995, Anklin et al. 1998, Kubon et al. 2002, Gao et al. 1994, Xu et al. 2000 and Xu et al. 2003).*

Figure 10 shows the results of all completed G_M^n experiments.

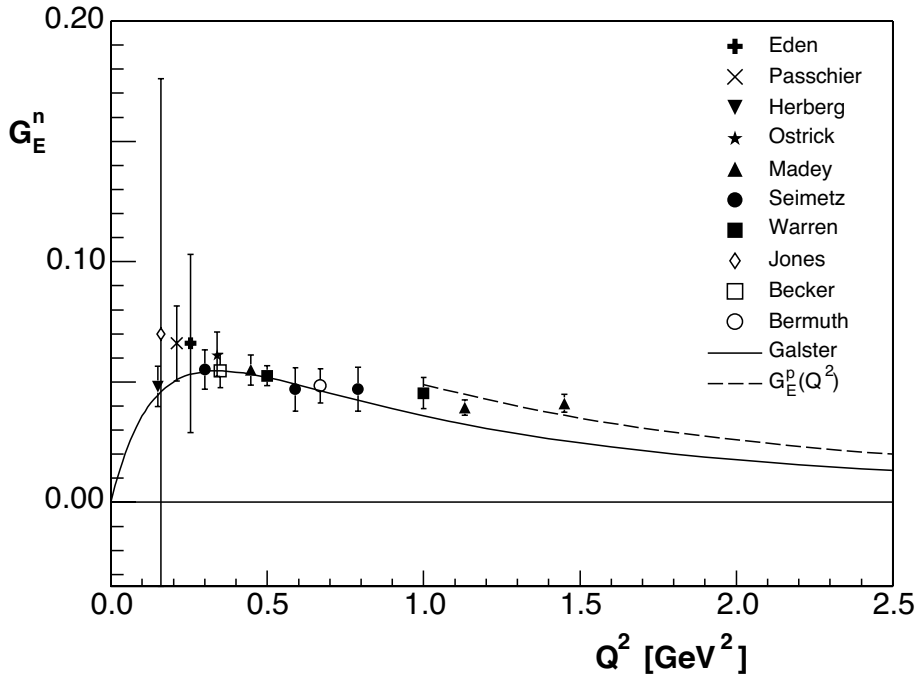

Figure 11. *The neutron electric form factor G_E^n as a function of Q^2. Results from $\vec{}^3\mathrm{He}$ are indicated by open symbols. Data are from References (Eden et al. 1994, Passchier et al. 1999, Herberg et al. 1999, Ostrick et al. 1999, Madey et al. 2003, Glazier et al. 2004, Warren et al. 2004, Jones et al. 1991, Becker et al. 1999, Golak et al. 2001 and Bermuth et al. 2003). The full curve shows the Galster (1971) parametrization; the dashed curve represents the Q^2-behavior of G_E^p.*

4.5 Neutron Electric Form Factor

Analogously to G_M^n, early G_E^n-experiments used (quasi-)elastic scattering off the deuteron to extract the longitudinal deuteron response function. Due to the smallness of G_E^n, the use of different nucleon-nucleon potentials resulted in a 100% spread in the resulting G_E^n values (Platchkov *et al.* 1990). In the past decade a series of double-polarization measurements of neutron knock-out from a polarized ^{2}H or ^{3}He target have provided accurate data on G_E^n. The ratio of the beam-target asymmetry with the target polarization perpendicular and parallel to the momentum transfer is directly proportional to the ratio of the electric and magnetic form factors,

$$\frac{G_E^n}{G_M^n} = -\frac{P_x}{P_z}\frac{E_e + E_e'}{2M}\tan(\frac{\theta_e}{2}), \tag{14}$$

where P_x and P_z denote the polarization component perpendicular and parallel to $\vec{q}$.

A similar result is obtained with an unpolarized deuteron target when one measures the polarization of the knocked-out neutron as a function of the angle over which the neutron

spin is precessed with a dipole magnet:

$$\frac{G_E^n}{G_M^n} = -\tan(\delta)\sqrt{\frac{\tau(1+\epsilon)}{2\epsilon}}; \tag{15}$$

here, δ denotes the precession angle where the measured asymmetry is zero.

Again, the first such measurements were carried out at Bates, both with a polarized $^3\vec{\mathrm{He}}$ target and with a neutron polarimeter. Figure 11 shows results obtained through all three reactions $^2\vec{\mathrm{H}}(\vec{e},e'n)$, ^{2}H$(\vec{e},e'\vec{n})$ and $^3\vec{\mathrm{He}}(\vec{e},e'n)$. At low Q^2-values corrections for nuclear medium and rescattering effects can be sizeable: 65% for ^{2}H at 0.15 GeV^2 and 50% for ^{3}He at 0.35 GeV^2. These corrections are expected to decrease significantly with increasing Q, although no reliable calculations are presently available for ^{3}He above 0.5 GeV^2. There is excellent agreement between the results from the different techniques. Moreover, medium effects have clearly become negligible at $\sim$ 0.7 GeV^2, even for ^{3}He. The latest data from Hall C at Jefferson Lab, using either a polarimeter or a polarized target (Madey *et al.* 2003, Warren *et al.* 2004), extend up to $Q^2 \approx$ 1.5 GeV^2 with an overall accuracy of $\sim$10%, in mutual agreement. From $\sim$ 1 GeV^2 onwards G_E^n appears to exhibit a Q^2-behavior similar to that of G_E^p. Schiavilla and Sick (2001) have extracted G_E^n from available data on the deuteron quadrupole form factor $F_{C2}(Q^2)$ with a much smaller sensitivity to the nucleon-nucleon potential than from inclusive (quasi-)elastic scattering. The 30-years-old Galster parametrization (Galster *et al.* 1971) continues to provide a fortuitously good description of the data.

4.6 Timelike Form Factors

In the timelike region EMFF measurements have been made at electron-positron storage rings or by studying the inverse reaction (only for the proton form factors), antiproton annihilation on a hydrogen target. The rather limited data set on timelike form factors is shown in Figure 12. The quality of the data does not allow a separation of the charge and magnetic form factors; G_M has been extracted from the data using the G_E-values calculated by Iachello and Wan (2004). Clearly G_D which gives a very good description of the spacelike magnetic form factors, does not describe the data in the timelike region, at least from threshold down to -6 GeV^2. Iachello and Wan (2004), Hammer *et al.* (1996) and Dubnicka *et al.* (2003) have carried out an analytic continuation of their VMD calculations (section 5). Iachello's model provides a consistent description of the magnetic form factors in the timelike region. An extension of the data set in the timelike region and of theoretical efforts to obtain a consistent description of all EMFFs in both the space- and timelike regions is highly desirable.

4.7 Experimental Review and Outlook

In recent years highly accurate data on the nucleon EMFFs have become available from various facilities around the world, made possible by the development of high luminosity and novel polarization techniques. These have established some general trends in the Q^2-behavior of the four EMFFs. The two magnetic form factors G_M^p and G_M^n are close

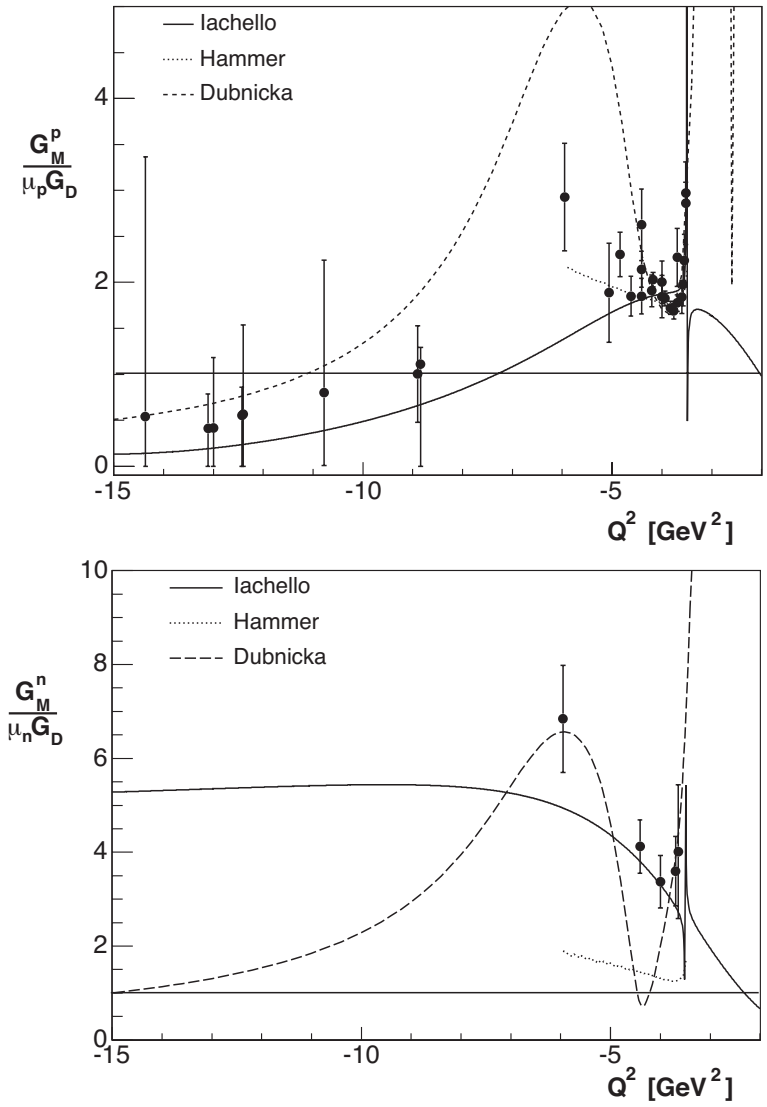

Figure 12. *The magnetic form factors (divided by G_D) in the time-like region as a function of Q^2, compared to the calculations by Iachello and Wan (2004), Hammer et al. (1996) and Dubnicka et al. (2003). See Reference (Iachello and Wan 2004) for the references to the experimental data.*

to identical, following G_D to within 10% at least up to 5 GeV^2, with a shallow minimum at ~ 0.25 GeV^2 and crossing G_D at ~ 0.7 GeV^2. G_E^p/G_M^p drops linearly with Q^2 and G_E^n appears to drop from ~ 1 GeV^2 onwards at the same rate as G_E^p. Measurements that extend to higher Q^2-values and offer improved accuracy at lower Q^2-values, will become available in the near future. In Hall C at Jefferson Lab Perdrisat *et al.* (2001) will extend the measurements of G_E^p/G_M^p to 9 GeV^2 with a new polarimeter and large-

acceptance lead-glass calorimeter. Wojtsekhowski *et al.* (2002) will measure G_E^n in Hall A at Q^2-values of 2.4 and 3.4 GeV^2 using the $^3\vec{\rm He}(\vec{e},e'n)$ reaction with a 100 msr electron spectrometer. The Bates Large Acceptance Spectrometer Toroid facility (BLAST, http://www.mitbates.mit.edu) at MIT with a polarized hydrogen and deuteron target internal to a storage ring will provide highly accurate data on G_E^p and G_E^n in a Q^2-range from 0.1 to 0.8 GeV^2. Gao *et al.* (2001) have shown that the proton charge radius can be measured with unprecedented precision by measuring the ratio of asymmetries in the two sectors of the BLAST detector. Thus, within a couple of years G_E^n data with an accuracy of 10% or better will be available up to a Q^2-value of 3.4 GeV^2. Once the upgrade to 12 GeV (Cardman *et al.* 2004) has been implemented at Jefferson Lab, it will be possible to extend the data set on G_E^p and G_M^n to 14 GeV^2 and on G_E^n to 5 GeV^2.

The charge and magnetization rms radii are related to the form-factor slope at Q^2= 0:

$$< r_E^2 >= \int \rho(r) r^4 dr = -6 \frac{dG(Q^2)}{dQ^2}\Big|_{Q^2=0}$$
$$< r_M^2 >= \int \mu(r) r^4 dr = -\frac{6}{\mu} \frac{dG(Q^2)}{dQ^2}\Big|_{Q^2=0}, \qquad (16)$$

with ρ(r) (μ(r)) denoting the radial charge (magnetization) distribution. Table 1 lists the results. For an accurate extraction of the radius Sick (2003) has shown that it is necessary to take into account Coulomb distortion effects and higher moments of the radial distribution. His result for the proton charge radius is in excellent agreement with the most recent three-loop QED calculation (Melnikov and Van Ritbergen 2000) of the hydrogen Lamb shift. Within error bars the rms radii for the proton charge and magnetization distribution and for the neutron magnetization distribution are equal. The value for the neutron charge radius was obtained (Kopecky *et al.* 1997) by measuring the transmission of low-energy neutrons through liquid ^{208}Pb and ^{209}Bi. The Foldy term $\frac{3}{2}\frac{\kappa}{M_n^2} = -0.126$ fm^2 is close to the value of the neutron charge radius. Isgur (1999) showed that the Foldy term is canceled by a first-order relativistic correction, which implies that the measured value of the neutron charge radius is indeed dominated by its internal structure.

Table 1. *Values for the nucleon charge and magnetization radii*

Observable	**value $\pm$ error**	**Reference**
$< (r_E^p)^2 >^{1/2}$	0.895 $\pm$ 0.018 fm	(Sick 2003)
$< (r_M^p)^2 >^{1/2}$	0.855 $\pm$ 0.035 fm	(Sick 2003)
$< (r_E^n)^2 >$	- 0.119 $\pm$ 0.003 fm^2	(Kopecky *et al.* 1997)
$< (r_M^n)^2 >^{1/2}$	0.87 $\pm$ 0.01 fm	(Kubon *et al.* 2002)

In the Breit frame the nucleon form factors can be written as Fourier transforms of their charge and magnetization distributions. However, if the wavelength of the probe is larger than the Compton wavelength of the nucleon, i.e. if $|Q| \geq M_N$, the form factors are not solely determined by the internal structure of the nucleon. Then, they also contain dy-

namical effects due to relativistic boosts and consequently the physical interpretation of the form factors becomes complicated. Recently, Kelly (2002) has extracted spatial nucleon densities from the available form factor data. He selected a model for the Lorentz contraction of the Breit frame in which the asymptotic behavior of the form factors conformed to perturbative quantum chromo-dynamics (pQCD) scaling at large Q^2-values and expanded the densities in a complete set of radial basis functions, with constraints at large radii. The neutron and proton magnetization densities are found to be quite similar, narrower than the proton charge density. He reports a neutron charge density with a positive core surrounded by a negative surface charge, peaking at just below 1 fm, which he attributes to a negative pion cloud. Alternatively, he extracts the radial distributions of the u and d quarks which both show a secondary lobe which he interprets as an indication of an orbital angular momentum (OAM) component in the quark distributions. Friedrich and Walcher (2003) observe a bump/dip at $Q \approx 0.5$ GeV with a width of ~ 0.2 GeV, a feature common to all EMFFs . A fit to all four EMFFs was performed, assuming a dipole behaviour for the form factors of the constituent quarks and an $l = 1$ harmonic oscillator behaviour for that of the pion cloud. They then transformed their results to coordinate space, neglecting the Lorentz boost, where they find that the pion cloud peaks at a radius of ~ 1.3 fm, slightly larger than Kelly did, close to the Compton wavelength of the pion. Hammer *et al.* (2004) argue from general principles that the pion cloud should peak much more inside the nucleon, at ~ 0.3 fm. However, they assign the full $N\bar{N}2\pi$ continuum to the pion cloud which includes different contributions than just the one-pion loop that Kelly (and Friedrich and Walcher) assign to the pion cloud. The structure at ~ 0.5 GeV, common to all EMFFs, is at such a small Q^2-value that its transformation to coordinate space should be straightforward.

5 Model Calculations

The recent production of very accurate EMFF data, especially the surprising G_E^p data from polarization transfer, has prompted the theoretical community to intensify their investigation of nucleon structure. Space limitations compel us to focus on only a few highlights. The interested reader is encouraged to read the original publications; the review by Thomas and Weise (2001) is an excellent introduction.

The u-, d- and s-quarks are the main building blocks of the nucleon in the kinematic domain relevant to this review. Its basic structure involves the three lightest vector mesons (ρ, ω and ϕ) which have the same quantum numbers as the photon. Consequently, one should expect these vector mesons to play an important role in the interaction of the photon with a nucleon. The first EMFF models were based on this principle, called vector meson dominance (VMD), in which one assumes that the virtual photon - after becoming a quark-antiquark pair - couples to the nucleon as a vector meson. The EMFFs can then be expressed in terms of coupling strengths between the virtual photon and the vector meson and between the vector meson and the nucleon, summing over all possible vector mesons. In the scattering amplitude a bare-nucleon form factor is multiplied by the amplitude of the photon interaction with the vector meson. With this model Iachello *et al.* (1973) predicted a linear drop of the proton form factor ratio, similar to that measured by polarization transfer, more than 20 years before the data became available. Gari and Krümpelmann (1985) extended the VMD model to conform with pQCD scaling at large

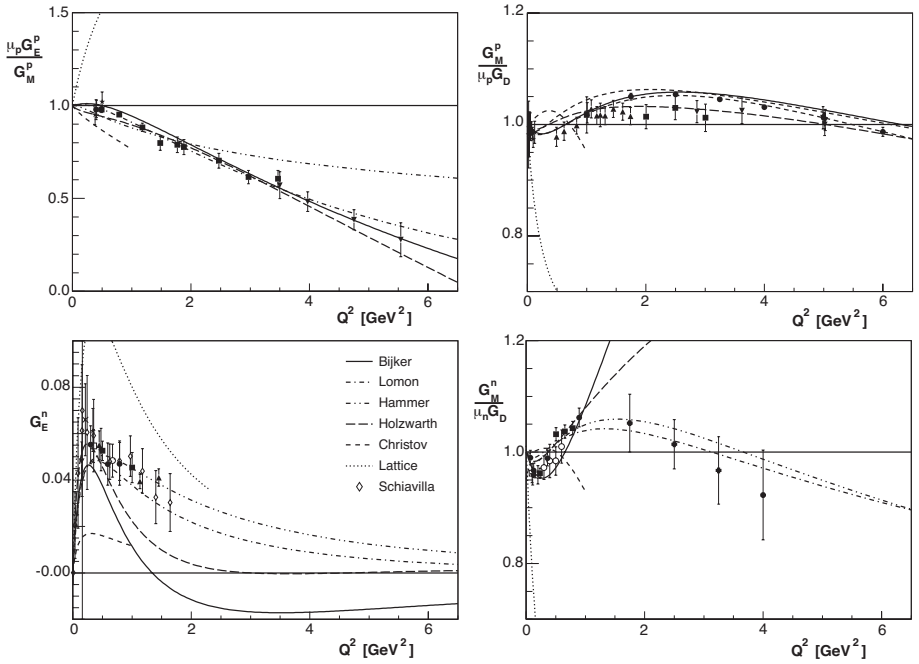

Figure 13. *Comparison of various calculations with available EMFF data, indicated by the same symbols as in Figures 7, 9, 10 and 11. For G_E^p only polarization-transfer data are shown. Not shown are the data for G_E^n of References (Jones et al. 1991 and Eden et al. 1994) and the data for G_M^n of References (Rock et al. 1992, Arnold et al. 1988, Markowitz et al. 1993, Gao et al. 1994, Bruins et al. 1995). For G_E^n the results of Schiavilla and Sick (2001) have been added. The calculations shown are from References (Bijker and Iachello 2004, Lomon 2001, Hammer and Meissner 2004, Holzwarth 1996, Christov et al. 1995 and Ashley 2004). Where applicable, the calculations have been normalized to the calculated values of $\mu_{p,n}$.*

Q^2-values. The VMD picture is not complete, as becomes obvious from the fact that the Pauli isovector form factor F_2^V is much larger than the isoscalar one F_2^S. An improved description requires the inclusion of the isovector $\pi\pi$ channel through dispersion relations (Höhler *et al.* 1976, Mergell *et al.* 1996). By adding more parameters, such as the width of the ρ-meson and the masses of heavier vector mesons (Lomon 2001), the VMD models succeeded in describing new EMFF data as they became available, but with little predictive power. Figure 13 confirms that Lomon's calculations provide an excellent description of all EMFF data. Bijker and Iachello (2004) have extended the original calculations by also including a meson-cloud contribution in F_2, but still taking only two isoscalar and one isovector poles into account. The intrinsic structure of the nucleon is estimated to have an rms radius of ~ 0.34 fm. These new calculations are in good agreement with the proton form-factor data, but do rather poorly for the neutron. The most recent dispersion-theoretical analysis (Hammer *et al.* 2004), using four isoscalar and three isovector mesons, results in an excellent description of G_M^p and G_M^n, but only reasonably describes G_E^p and G_E^n. Subsequent studies (Fuchs *et al.* 2004) have further

developed this combined approach to include chiral perturbation theory. However, such models can only be used at small Q^2-values, ≤ 0.4 GeV^2.

Many recent theoretical studies of the EMFFs have applied various forms of a relativistic constituent quark model (RCQM). Nucleons are assumed to be composed of three constituent quarks, which are quasi-particles where all degrees of freedom associated with the gluons and $q\bar{q}$ pairs are parametrized by an effective mass. Because the momentum transfer can be several times the nucleon mass, the constituent quarks require a relativistic quantum-mechanical treatment. Three possibilities exist for such a treatment: the instant form, where the interaction is present in the time component of the four-momentum and in the Lorentz boost; the point form, where all components of the four-momentum operator depend on the interaction; and the light-front form, where the interaction appears in one component of the four-momentum and in the transverse rotations. In each of these forms the Poincaré invariance can be broken in the number of constituents (by the creation of $q\bar{q}$ pairs) or by the use of approximate current operators. Although most of these calculations correctly describe the EMFF behaviour at large Q^2-values, effective degrees of freedom, such as a pion cloud and/or a finite size of the constituent quarks, are introduced to correctly describe the behaviour at lower Q^2-values.

Miller (2002a) uses an extension of the cloudy bag model (Théberge 1981), three relativistically moving (in light-front kinematics) constituent quarks, surrounded by a pion cloud. He chose a spatial wave function, as derived by Schlumpf (1994), whose parameters (and those of the pion cloud) are chosen to describe the magnetic moments, the neutron charge radius, and the EMFF behavior at large Q^2-values. Cardarelli and Simula (2000) also use light-front kinematics, but they calculate the nucleon wave function by solving the three-quark Hamiltonian in the Isgur-Capstick one-gluon-exchange potential. In order to get good agreement with the EMFF data they introduce a finite size of the constituent quarks in agreement (Petronzio *et al.* 2003) with recent DIS data. The results of Wagenbrunn *et al.* (Wagenbrunn *et al.* 2001) are calculated in a covariant manner in the point-form spectator approximation (PFSA). In addition to a linear confinement, the quark-quark interaction is based on Goldstone-boson exchange dynamics. The PFSA current is effectively a three-body operator (in the case of the nucleon as a three-quark system) because of its relativistic nature. It is still incomplete but it leads to surprisingly good results for the electric radii and magnetic moments of the other light and strange baryon ground states beyond the nucleon. Although Desplanques and Theussl 2003 have criticized the use of the point form in its introduction of two-body currents in the form of a neutral boson exchange, Coester and Riska (2003) obtain a reasonable representation of empirical form factors in this frame. Giannini *et al.* (2003) have explicitly introduced a three-quark interaction in the form of a gluon-gluon interaction in a hypercentral model, which successfully describes various static baryon properties. Relativistic effects are included by boosting the three quark states to the Breit frame and by introducing a relativistic quark current. All previously described RCQM calculations used a non-relativistic treatment of the quark dynamics, supplemented by a relativistic calculation of the electromagnetic current matrix elements. Merten *et al.* (2002) have solved the Bethe-Salpeter equation with instantaneous forces, inherently respecting relativistic covariance. In addition to a linear confinement potential, they used an effective flavor-dependent two-body interaction. For static properties this approach yields results caut similar to those obtained by Wagenbrunn *et al.* (2001). The results of these five

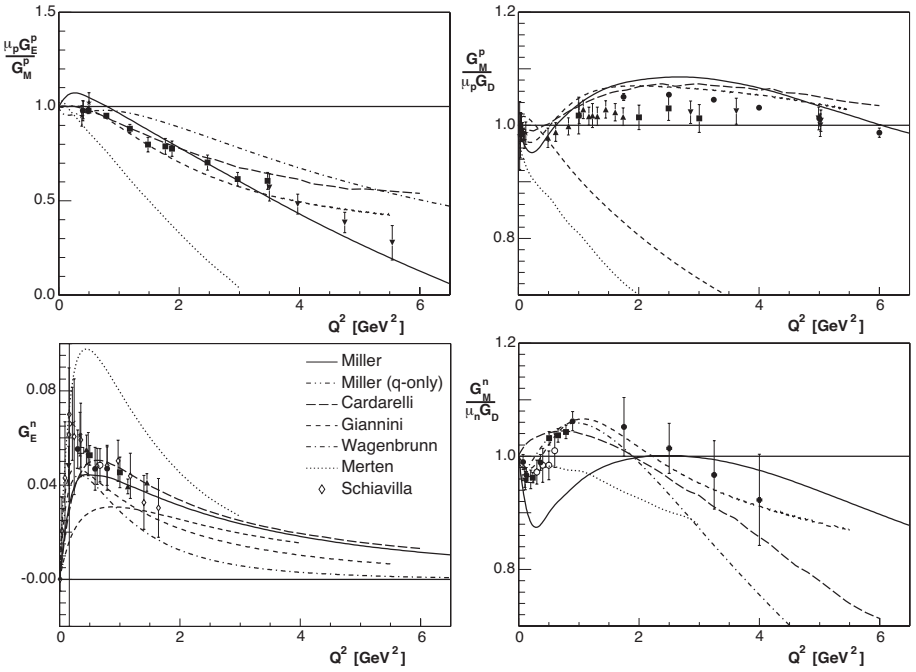

Figure 14. *Comparison of various RCQM calculations with available EMFF data, similar to the comparison in Figure 13. The calculations shown are from References (Miller 2002a, Cardarelli and Simula 2000, Giannini et al. 2003, Wagenbrunn et al. 2001 and Merten et al. 2002). Miller (q-only) denotes a calculation by Miller (2002a) in which the pion cloud has been suppressed. Where applicable, the calculations have been normalized to the calculated values of* $\mu_{p,n}$.

calculations are compared to the EMFF data in Figure 14. The calculations of Miller do well for all EMFFs, except for G_M^n at low Q^2-values. Those of Cardarelli and Simula, Giannini *et al.* and Wagenbrunn *et al.* are in reasonable agreement with the data, except for that of Wagenbrunn *et al.* for G_M^p, while the results of Merten *et al.* provide the poorest description of the data.

Before the Jefferson Lab polarization transfer data on G_E^p/G_M^p became available Holzwarth (1996) predicted a linear drop in a chiral soliton model. In such a model the quarks are bound in a nucleon by their interaction with chiral fields. In the bare version quarks are eliminated and the nucleon becomes a skyrmion with a spatial extension, but the Skyrme model provided an inadequate description of the EMFF data. Holzwarth's extension introduced one vector-meson propagator for both isospin channnels in the Lagrangian and a relativistic boost to the Breit frame. His later calculations used separate isovector and isoscalar vector-meson form factors. He obtained excellent agreement for the proton data, but only a reasonable description of the neutron data. Christov *et al.* (1995) used an SU(3) Nambu-Jona-Lasinio Lagrangian, an effective theory that incorporates spontaneous chiral symmetry breaking. This procedure is comparable to the inclusion of vector mesons into the Skyrme model, but it involves many fewer free parameters (which are

fitted to the masses and decay constants of pions and kaons). The calculations are limited to $Q^2 \leq 1$ GeV^2 because the model is restricted to Goldstone bosons and because higher-order terms, such as recoil corrections, are neglected. A constituent quark mass of 420 MeV provided a reasonable description of the EMFF data (Figure 13).

In the asymptotically free limit, QCD can be solved perturbatively, providing predictions for the EMFF behavior at large Q^2-values. Brodsky and Farrar (1975) derived a scaling law for the Pauli and Dirac form factors based on a dimensional analysis, that entailed counting propagators and the number of scattered constituents:

$$F_1 \propto (Q^2)^{-2}, \quad F_2 \propto (Q^2)^{-3}, \quad F_2/F_1 \propto Q^{-2} \tag{17}$$

Brodsy and Lepage (1981) later reached the same asymptotic behavior based on a more detailed theory that assumed factorization and hadron helicity conservation. The recent polarization transfer data clearly do not follow this pQCD prediction (which the Rosenbluth data unfortunately do). Miller (2002b) was the first to observe that imposing Poincaré invariance removes the pQCD condition that the transverse momentum must be zero, and introduces a quark OAM component in the wavefunction of the proton, thus violating hadron helicity conservation. His model predicts a $1/Q$ behaviour for the ratio of the Dirac and Pauli form factors at intermediate Q^2-values, in excellent agreement with the polarization transfer data for $Q^2 \geq 3$ GeV^2. Iachello and Wan (2004) and others have pointed out that this $1/Q$ behaviour is accidental and only valid in an intermediate Q^2-region. Ralston and Jain (2004) has generalized this issue to conclude that the Q^2-behavior of the Jefferson Lab data signals substantial quark OAM in the proton. Recently, Brodsky *et al.* (2004) and Belitsky *et al.* (2003) have independently revisited the pQCD domain. Belitsky *et al.* derive the following large Q^2-behavior:

$$\frac{F_2}{F_1} \propto \frac{\ln^2 Q^2/\Lambda^2}{Q^2}, \tag{18}$$

where Λ is a soft scale related to the size of the nucleon. Even though the Jefferson Lab data follow this behavior (Figure 15), Belitsky *et al.* warn that this could very well be precocious, since pQCD is not expected to be valid at such low Q^2-values. Brodsky *et al.* (2004) argue that a nonzero OAM wave function should contribute to both F_1 and F_2 and that thus Q^2F_2/F_1 should still be asymptotically constant.

Once enough data have been collected on generalized parton distributions, it will become possible to construct a three-dimensional picture of the nucleons, with the three dimensions being the two transverse spatial coordinates and the longitudinal momentum. Miller (2003) has further investigated the information that can be extracted from form-factor data by themselves. His colorful images of the proton should be interpreted as three-dimensional pictures of the proton as a function of the momentum of the quark, probed by the virtual photon, and for different orientations of the spin of that quark relative to that of the proton. Ji (2003) has derived similar images from generalized parton distributions using Wigner correlation functions for the quark and gluon distributions.

However, all theories described until now are at least to some extent effective (or parametrizations). They use models constructed to focus on certain selected aspects of QCD. Only lattice gauge theory can provide a truly ab initio calculation, but accurate lattice QCD

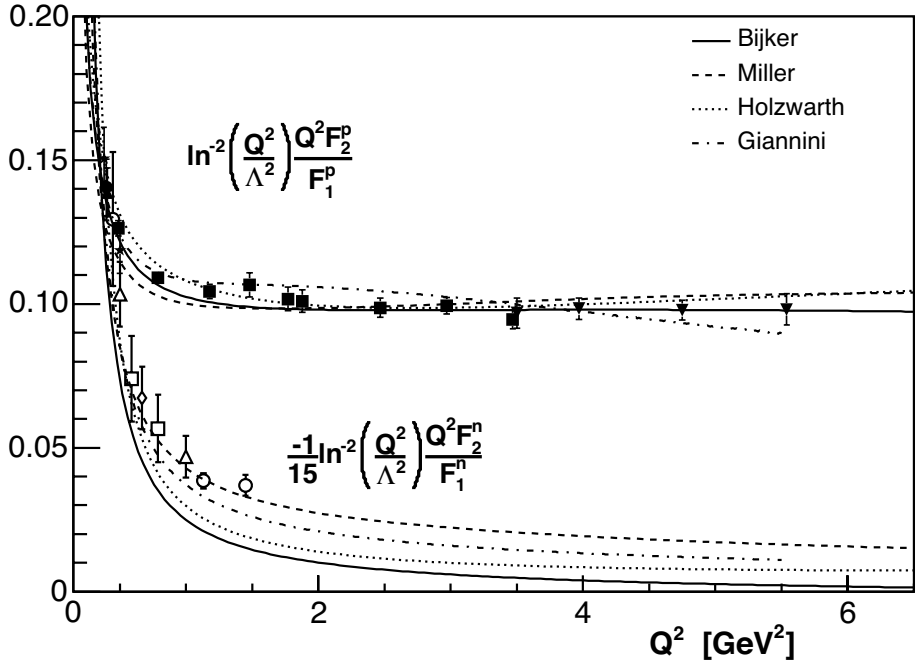

Figure 15. *The ratio $(Q^2F_2/F_1)/\ln^2(Q^2/\Lambda^2)$ as a function of Q^2 for the polarization-transfer data and the calculations of References (Bijker and Iachello 2004, Miller 2002a, Holzwarth 1996 and Giannini et al. 2003). The same ratio, scaled by a factor -1/15, is shown for the neutron with open symbols. For Λ a value of 300 MeV has been used.*

results for the EMFFs are still several years away. One of the most advanced lattice calculations of EMFFs has been performed by the QCDSF collaboration (Göckeler *et al.* 2003). The technical state of the art limits these calculations to the quenched approximation (in which sea-quark contributions are neglected), to a box size of 1.6 fm and to a pion mass of 650 MeV. Ashley *et al.* (2004) have extrapolated the results of these calculations to the chiral limit, using chiral coefficients appropriate to full QCD. The agreement with the data (Figure 13) is poorer than that of any of the other calculations, a clear indication of the technology developments required before lattice QCD calculations can provide a stringent test of experimental EMFF data.

6 Summary, Outlook and Conclusions

Recent advances in polarized electron sources, polarized nucleon targets and nucleon recoil polarimeters have enabled accurate measurements of the spin-dependent elastic electron-nucleon cross section. New data on nucleon electro-magnetic form factors with unprecedented precision have (and will continue to) become available in an ever increasing Q^2-domain. Highly accurate measurements with the Rosenbluth technique have established that the discrepancy between results on G_E^p/G_M^p with the Rosenbluth

techniques and with polarization transfer is not an instrumentation problem. Recent advances on two-photon exchange contributions make it highly likely that the application of TPE corrections will resolve that discrepancy. However, a continuing strong effort, both experimental and theoretical, is needed to firmly establish the applicability of TPE corrections.

The two magnetic form factors G_M^p and G_M^n closely follow the simple dipole form factor G_D. G_E^p/G_M^p drops linearly with Q^2 and G_E^n appears to drop at the same rate as G_E^p from $\sim$ 1 GeV^2 onwards. The Q^2-behavior of G_E^p has provided a signal of substantial non-zero orbital angular momentum in the proton. Only scant data are available in the time-like region. The full EMFF data set forms tight constraints on models of nucleon structure. So far, all available theories are at least to some extent effective (or parametrizations). Still, only few of these adequately describe all four EMFFs. Only lattice gauge theory can provide a truely ab initio calculation, but accurate lattice QCD results for the EMFFs are still several years away. A scaling prediction has been developed for the ratio of the Pauli and Dirac form factors, which the data appear to follow even at a Q^2-value as low as 1 GeV^2. Novel procedures allow a visualization of the nucleon structure as a function of the momentum of the struck quark. A fully three-dimensional picture of the nucleon will become available when future exclusive data have allowed the determination of the Generalized Parton Distributions.

I would like to conclude with a forty-years-old quote from the review by Wilson and Levinger (1964) which is still fully appropriate now: "Although the major landmarks of this field of study are now clear, we are left with the feeling that much is yet to be learned about the nucleon by refining and extending both measurement and theory."

Acknowledgements

The work presented was supported by the U. S. Department of Energy (DOE) contract DE-AC05-84ER40150 Modification NO. M175, under which the Southeastern Universities Research Association operates the Thomas Jefferson National Accelerator Facility.

References

Akhiezer AI, Rozentsweig LN and Shmushkevich IM, 1958, *Sov Phys JETP* **6** 588.
Alcorn J *et al.* , 2004, *Nucl Instrum Methods* **A522** 294.
Andivahis L *et al.* , 1994, *Phys Rev D* **50** 5491.
Anklin H *et al.* , 1994, *Phys Lett* **B336** 313.
Anklin H *et al.* , 1998, *Phys Lett* **B428** 248.
Arnold R, Carlson C and Gross F, 1981, *Phys Rev C* **23** 363.
Arnold R *et al.* , 1988, *Phys Rev Lett* **61** 806.
Arrington J, 2003, *Phys Rev C* **68** 034325.
Arrington J, 2004a, *Phys Rev C* **69** 022201R.
Arrington J, 2004b, *Phys Rev C* **69** 032201R and references therein.
Ashley JD *et al.* , 2004, *Eur Phys Jour A* **19 (Suppl. 1)** 9.
Aulenbacher K, 2002, *Proc. 9th Int. Workshop on Polarized Sources and Targets*, p. 141. Singapore: World Scientific.
Bartel W, *et al.* , 1966, *Phys Rev Lett* **17** 608.

Baylac M *et al.* , 2001, *Phys Lett* **B459** 412.
Becker J *et al.* , 1999, *Eur Phys Jour A* **6** 329.
Belitsky AV, Ji X and Yuan F, 2003, *Phys Rev Lett* **91** 092003.
Berger C, *et al.* , 1971, *Phys Lett* **B35** 87.
Bermuth J *et al.* , 2003, *Phys Lett* **B564** 199; Rohe D *et al.* , 1999, *Phys Rev Lett* **83** 4257.
Bijker R and Iachello F, 2004, *Phys Rev C* **69** 068201.
Blunden PG, Melnitchouk W and Tjon JA, 2003, *Phys Rev Lett* **91** 142304.
Borkowski F *et al.* , 1975, *Nucl Phys* **B93** 461.
Bosted PE *et al.* , 1990, *Phys Rev C* **42** 38.
Bosted P, et al. 1995, *Phys Rev C* **51** 409.
Brash E *et al.* , 2002, *Phys Rev C* **65** 051001.
Brodsky SJ and Farrar G, 1975, *Phys Rev D* **11** 1309.
Brodsky SJ and Lepage GP, 1981, *Phys Rev D* **24** 2848.
Brodsky SJ *et al.* , 2004, *Phys Rev D* **69** 076001.
Brooks W and Vineyard MF, 1994, spokespersons, Jefferson Lab experiment E94-017; private communication.
Brooks W *et al.* , 2004, spokespersons, Jefferson Lab experiment E-04-116.
Bruins EEW *et al.* , 1995, *Phys Rev Lett* **75** 21.
Cardarelli F and Simula S, 2000, *Phys Rev C* **62** 065201.
Cardman LS *et al.* , editors, 2003, *Pre-Conceptual Design Report for the Science and Experimental Equipment for the 12 GeV Upgrade of CEBAF*,
http://www.jlab.org/div_dept/physics_division/pCDR_public/pCDR_final.
Chen YC *et al.* , 2004, *Phys Rev Lett* **93** 122301.
Christov CV *et al.* , 1995, *Nucl Phys* **A592** 513; Kim HC *et al.* , 1996, *Phys Rev D* **53** 4013.
Christy ME *et al.* , 2004, nucl-ex/0401030.
Chudakov E and Luppov V, 2004, *IEEE Trans on Nucl Science*, **51**, 1533.
Clasie B *et al.* , 2003, *Presented at X-th Workshop on Polarized Sources and Targets*, Novosibirsk.
Coester F and Riska DO, 2003, *Nucl Phys* **A728** 439.
Crabb D *et al.* , 1995, *Nucl Instrum Methods* **A356** 9; Averett TD *et al.* , 1999, *Nucl Instrum Methods* **A427** 440.
Derbenev YaS and Kondratenko AM, 1973, *Sov Phys JETP* **37** 968.
Desplanques B and Theussl L, 2003, hep-ph/0307028.
Dieterich S *et al.* , 2001, *Phys Lett* **B500** 47.
Donnelly TW and Raskin AS, 1986, *Ann Phys, NY* **169** 247.
Dubnicka S, Dubnickova AZ and Weisenpacher P, 2003, *J Phys G: Nucl Part Phys* **29** 405.
Eden T *et al.* , 1994, *Phys Rev C* **50** R1749.
Friedrich J and Walcher Th, 2003, *Eur Phys Jour A* **17** 607.
Frisch R and Stern O, 1933, *Z Phys* **85** 4; Estermann I and Stern O, 1933, *Z Phys* **85** 17.
Fuchs T, Gegelia J and Scherer S, 2004, *Eur Phys Jour A* **19 (Suppl. 1)** 35 and references therein.
Galster S *et al.* , 1971, *Nucl Phys* **B32** 221.
Gao H *et al.* , 1994, *Phys Rev C* **50** R546.
Gao H, Calarco JR and Kolster H, 2001, spokespersons. MIT-Bates proposal 01-01.
Gari MF and Krümpelmann W, 1985, *Z Phys* **A322** 689; 1992, *Phys Lett* **B274** 159.
Gayou O *et al.* , 2002, *Phys Rev Lett* **88** 092301.
Giannini M, Santopinto E and Vassallo A, 2003, *Prog Part Nucl Phys* **50** 263; De Sanctis M *et al.* , 2000, *Phys Rev C* **62** 025208; Ferraris M *et al.* , 1995, *Phys Lett* **B364** 231.
Glazier D *et al.* , 2004, nucl-ex/0410026, submitted to *Eur Phys Jour A*.
Göckeler M *et al.* , 2003, hep-lat/0303019.
Golak J *et al.* , 2001, *Phys Rev C* **63** 034006.
Guichon PAM and Vanderhaeghen M, 2003, *Phys Rev Lett* **91** 142303.
Hammer HW, Meissner UG and Drechsel D, 1996, *Phys Lett* **B385** 343.

Hammer HW and Meissner UG, 2004, *Eur Phys Jour A* **20** 469.
Hammer HW, Drechsel D and Meissner UG, 2004, *Phys Lett* **B586** 291.
Hand LN, Miller DG and Wilson R, 1963, *Rev Mod Phys* **35** 335.
Hauger M *et al.* , 2001, *Nucl Instrum Methods* **A462** 382.
Herberg C *et al.* , 1999, *Eur Phys Jour A* **5** 131.
Höhler G *et al.* , 1976, *Nucl Phys* **B114** 505.
Holzwarth G, 1996, *Z Phys* **A356** 339; hep-ph/0201138.
Iachello F, Jackson A and Lande A, 1973, *Phys Lett* **B43** 191.
Iachello F and Wan Q., 2004, *Phys Rev C* **69** 055204.
Isgur N, 1999, *Phys Rev Lett* **83** 272.
Janssens T, *et al.* , 1966, *Phys Rev* **142** 922.
Ji X, 2003, *Phys Rev Lett* **91** 062001.
Jones-Woodward CE *et al.* , 1991, *Phys Rev C* **44** R571.
Kelly JJ, 2002, *Phys Rev C* **66** 065203.
Kopecky S *et al.* , 1997, *Phys Rev C* **56** 2229.
Kubon G *et al.* , 2002, *Phys Lett* **B524** 26.
Litt J, *et al.* , 1970, *Phys Lett* **B31** 40 and references therein.
Lomon EL, 2001, *Phys Rev C* **64** 035204; 2002, *Phys Rev C* **66** 045501.
Lung AF *et al.* , 1993, *Phys Rev Lett* **70** 718.
Madey R *et al.* , 2003, *Phys Rev Lett* **91** 122002.
Markowitz P *et al.* , 1993, *Phys Rev C* **48** R5.
Melnikov K and van Ritbergen T, 2000, *Phys Rev Lett* **84** 1673.
Mergell P, Meissner UG and Drechsel D, 1996, *Nucl Phys* **A596** 367.
Merten D *et al.* , 2002, *Eur Phys Jour A* **14** 477.
Milbrath B *et al.* , 1998, *Phys Rev Lett* **80** 452; erratum, 1999, *Phys Rev Lett* **82** 2221.
Miller GA, 2002a, *Phys Rev C* **66** 032001R.
Miller GA, 2002b, *Phys Rev C* **65** 065205.
Miller GA, 2003, *Phys Rev C* **68** 022201R.
Mo LW and Tsai YS, 1969, *Rev Mod Phys* **41** 205; Maximon LC and Tjon JA, 2000, *Phys Rev C* **62** 054320.
Offermann EAJM *et al.* , 1991, *Phys Rev C* **44** 1096.
Ostrick M *et al.* , 1999, *Phys Rev Lett* **83** 276.
Passchier I *et al.* , 1999, *Phys Rev Lett* **82** 4988.
Perdrisat CF *et al.* , 2001, spokespersons, Jefferson Lab experiment E01-109.
Petronzio R, Simula S and Ricco G, 2003, *Phys Rev D* **67** 094004.
Platchkov S *et al.* , 1990, *Nucl Phys* **A510** 740.
Pospischil T *et al.* , 2001, *Eur Phys Jour A* **12** 125.
Punjabi V *et al.* , 2003, submitted to *Phys Rev C*; Jones MK *et al.* , 2000, *Phys Rev Lett* **84** 1398.
Qattan IA *et al.* , 2004, nucl-ex/0410010, submitted to *Phys Rev Lett*.
Ralston JP and Jain P, 2004, *Phys Rev D* **69** 053008.
Rock S *et al.* , 1992, *Phys Rev D* **46** 24.
Rosenbluth MN, 1950, *Phys Rev* **79** 615.
Sargsian M, 2001, *Int J Mod Phys* **E 10** 405.
Schiavilla R and Sick I, 2001, *Phys Rev C* **64** 041002.
Schlumpf F, 1994, *J Phys G: Nucl Part Phys* **20** 237.
Sick I, 2003, *Phys Lett* **B576** 62; private communication (2004).
Sill AF *et al.* , 1993, *Phys Rev D* **48** 29.
Steffens E and Haeberli W, 2003, *Rep Prog Phys* **66** 1887.
Steigerwald M, 2001, *Proc. 14th Int. Workshop on Polarized Sources*, AIP Conference Proceedings vol. 570, p. 935. New York: American Institute of Physics.
Surkau R *et al.* , 1997, *Nucl Instrum Methods* **A384** 444.

Théberge S, Thomas AW and Miller GA, 1981, *Phys Rev D* **24** 216.
Thomas AW and Weise W, 2001, *The Structure of the Nucleon*, Berlin: Wiley-VCH.
Van Cauteren T *et al.* , 2004, *Eur Phys Jour A* **20** 283.
Wagenbrunn RF *et al.* , 2001, *Phys Lett* **B511** 33; Boffi S *et al.* , 2002, *Eur Phys Jour A* **14** 17.
Walker RC *et al.* , 1994, *Phys Rev D* **49** 5671.
Warren G *et al.* , 2004, *Phys Rev Lett* **92** 042301; Zhu H *et al.* , 2001, *Phys Rev Lett* **87** 081801.
Wilson RR and Levinger JS, 1964, *Ann Rev Nucl Science* **14** 135.
Wojtsekhowski B *et al.* , 2002, spokespersons, Jefferson Lab experiment E02-013.
Xu W *et al.* , 2000, *Phys Rev Lett* **85** 2900.
Xu W *et al.* , 2003, *Phys Rev C* **67** 012201R.